# Fundamental Framework and Experiments of the Third Generation of IAP / LASG World Ocean General Circulation Model

Jin Xiangze (金向泽), Zhang Xuehong (张学洪)

*State Key Laboratory of Numerical Modeling for Atmospheric Sciences and Geophysical Fluid Dynamics (LASG), Institute of Atmospheric Physics, Chinese Academy of Sciences, Beijing 100080*

Zhou Tianjun (周天军)

*Department of Geophysics, Peking University, Beijing 100871*

(Received June 8, 1998; revised September 8, 1998)

ABSTRACT

A new generation of the IAP / LASG world ocean general circulation model is designed and presented based on the previous 20-layer model, with enhanced spatial resolutions and improved parameterizations. The model uses a triangular-truncated spectral horizontal grid system with its zonal wave number of 63 (T63) to match its atmospheric counterpart of a T63 spectral atmosphere general circulation model in a planned coupled ocean-atmosphere system. There are 30 layers in vertical direction, of which 20 layers are located above 1000 m for better depicting the permanent thermocline. As previous ocean models developed in IAP / LASG, a free surface (rather than "rigid-lid" approximation) is included in this model. Compared with the 20-layer model, some more detailed physical parameterizations are considered, including the along / cross isopycnal mixing scheme adapted from the Gent-MacWilliams scheme.

The model is spun up from a motionless state. Initial conditions for temperature and salinity are taken from the three-dimensional distributions of Levitus' annual mean observation. A preliminary analysis of the first 1000-year integration of a control experiment shows some encouraging improvements compared with the twenty-layer model, particularly in the simulations of permanent thermocline, thermohaline circulation, meridional heat transport, etc. resulted mainly from using the isopycnal mixing scheme. However, the use of isopycnal mixing scheme does not significantly improve the simulated equatorial thermocline. A series of numerical experiments show that the most important contribution to the improvement of equatorial thermocline and the associated equatorial under current comes from reducing horizontal viscosity in the equatorial regions. It is found that reducing the horizontal viscosity in the equatorial Atlantic Ocean may slightly weaken the overturning rate of North Atlantic Deep Water.

**Key words:** Ocean general circulation model, Thermocline, Isopycnal mixing

## 1. Introduction

The first baroclinic oceanic general circulation model (OGCM) developed at the State Key Laboratory of Numerical Modeling for Atmospheric Sciences and Geophysical Fluid Dynamics (LASG), Institute of Atmospheric Physics (IAP) is a four-layer model with its horizontal resolution of $4^\circ \times 5^\circ$, covering the scope from 60°S to 60°N (Zhang et al., 1989). The model was further improved (Zhang et al., 1991) and successfully coupled with the two-level atmospheric general circulation model (AGCM) of Zeng et al. (1989) to study the interannual variability of climate (Zhang et al., 1992; Chen et al., 1993; Yu et al., 1995).

The second generation of IAP / LASG world ocean general circulation model is a twenty-layer model (ML20) with the same horizontal resolution as that of the four-layer model but covering from the Antarctic continent coastline to 70°N in its original version (Chen, 1994; Zhang et al., 1996, hereafter referred as ML20-0) and the global scope except the North Pole in its revised version (Yu, 1997, hereafter referred as ML20-1). Another important difference between ML20-0 and ML20-1 is that the former uses the "upwind" tracer-advection scheme (Maier-Reimer et al., 1993) without explicit diffusion terms, but the latter uses the central finite-difference advection scheme and has conventional second-order diffusion terms. With fairly successful simulation of thermohaline circulation, ML20-0 was coupled with the two-level AGCM to study mean climate (Guo et al., 1996) and climate change (Chen et al., 1997). Afterwards, ML20-1 was coupled with the nine-layer spectral AGCM of Wu et al. (1996) by Liu et al. (1996) and Yu (1997) to provide a framework for the global ocean-atmosphere-land system model (GOALS / LASG, see Wu et al., 1997).

Since the late 1996, an effort in developing the third generation of the IAP / LASG world ocean general circulation model was initiated by the authors based on knowledge and experience gained from the previous ocean modeling activities and from the increasing interactions with other climate modeling communities in the world. The direct motivation for the effort is to meet the requirement of developing higher-resolution and higher-accuracy large-scale global ocean models, as one of the important components of the "National Key Project Studies on Short-range Climate Prediction System in China" and the "National Climbing Project Studies on Climate Dynamics and Climate Prediction Theory". It is recognized that the development of oceanic general circulation models must involve in a continually improving / updating process. Therefore, we began the work with reconstructing ML20 within a higher spatial resolution framework and changing just a few selected physical processes. In comparison with ML20, the most important improvements in the newly developed model lie in the following two aspects.

First, the spatial resolutions in both horizontal and vertical in the present model are remarkably enhanced (although the model should still fall into the category of "coarse-resolution" models) on the basis of the greatly increased computer resources in IAP / LASG since 1997. The horizontal discretization is conducted based on a triangular spectral truncation with its zonal wave number of 63 (T63), which approximates to a grid size of about $1.875° \times 1.875°$. One of the reasons for choosing the T63 horizontal resolution can be found in Covey (1994) who pointed out that changes in large-scale circulation and heat transport are obvious when grid spacing decreases especially from 4° to 2°. Moreover, since the model will be coupled with a T63 AGCM (Dong et al., personal communication), an identical grid system may help diminishing loss of accuracy in ocean-atmosphere data exchange processes.

Second, some fairly mature parameterization schemes are adopted to this model. These include the penetration of solar radiation (Rosati et al., 1988); the Richardson number-dependent mixing process in the equatorial oceans; a more detailed parameterization of air-sea heat exchange in areas with leads; and the along isopycnal and isopycnal thickness mixing scheme of Gent and MacWilliams (1990, referred as GM90). As reported by Dannabasoglu et al. (1994), with use of the GM90 scheme, they gained a great success in simulation of a sharper main thermocline, a larger meridional extent of the overturning cell with a strengthened northward heat transport in the Atlantic, and a more realistic convection in the open sea. These are of particular importance for the present model because that the two major problems in the performance of ML20 are considered as the simulated thermocline being too thick

and too diffuse, and the simulated outflow of the North Atlantic Deep Water (NADW) being too weak.

The paper is organized as follows. Brief descriptions of the present model and its fundamental experiments are given in Section 2. Some conventional analyses concerning the modeled mean upper ocean climate including sea surface temperature and salinity, surface height, and barotropic streamfunction are given in Section 3. Section 4 contributes to some major improvements in the simulated permanent thermocline, thermohaline circulation, and meridional heat transport achieved in the present model in comparison with both ML20 and observation. In addition to the permanent thermocline, a reasonable representation of the equatorial thermocline is also important due to its close relation with the ENSO dynamics. Some experiments have been designed and performed for improving the equatorial thermocline, which are described in Section 5. The last section (Section 6) is a summary.

## 2. Model and experiment descriptions

A brief description for various aspects of the present model, including dynamical framework, physical processes, computational design, and data sources for initial and boundary conditions, etc., is given in Table 1 which corresponds exactly to the basic experiment D2 as defined in Table 4. Those items written with black letters represent chief differences between the present model and ML20.

**Table 1.** Model description based on experiment D2

| | |
|---|---|
| Dynamics | Primitive eqs., Free surface (Zhang and Liang, 1989) |
| Sea Ice | Thermodynamic (Parkinson and Washington, 1979); Leads |
| **Resolution** | **T63 (Triangular spectral truncation, ~ 1.875° × 1.875°), L30 (30 layers, of which 20 in the upper 1000 m)** |
| Vertical Coordinates | ETA ($\eta$) (Mesinger and Janjic, 1975; Yu, 1989) |
| **Geography and Topography** | World ocean **(without including northward of 85.8°N** and Mediterranean Sea); **Modified bottom topography in the Arctic Sea; Data source: Scripps 1° × 1°** |
| **State Equation** | **Polynomial fitting to UNESCO (1981) based on Bryan and Cox (1972)** |
| ***Viscousity*** | **Horizontal: $20 \times 10^4$ $m^2/s$, Vertical: $10 \times 10^{-4}$ $m^2/s$** |
| **Diffusion** | **Isopycnal and isopycnal thickness diffusivities ($1.0 \times 10^3$ $m^2/s$), Backgrounnd vertical diffusivity ($0.3 \times 10^{-4}$ $m^2/s$), based on Gent and MacWilliams (1990)** |
| Finite-difference Scheme | Energy / Mass conserving (Zeng and Zhang, 1987); Multiple three-point smoother for high-latitudes |
| **Time Integration for Momentum Eqs.** | Separating-coupling for barotropic and baroclinic mode (Mellor, 1993); Asselin filter (Asselin, 1972). $\Delta t_B$ = 2 **min**, $\Delta t_C$ = 1 **h** |
| ***Time Integration for Tracers*** | ***Asynchronous with current field* (Bryan, 1984)**, $\Delta t_r$ = 24 h for all the layers |
| Convection Scheme | Marotzke (1991) |
| Type of Forcing | Seasonal cycle |
| Wind Stress | Hellerman and Rosenstein (1983) |
| ***Heat Flux*** | *Haney (1971)*, **Data source: COADS (da Silva et al., 1994)** |
| Fresh Water Flux | Replaced by restoring surface salinity to the observation of Levitus (1994) with a time-scale of 90 days |
| **Initial Conditions** | **Observed T / S of Levitus (1994)**, Motionless, and Flat sea surface |

**Table 2.** Global and annual mean temperatures in °C for the year 1000 and its centennial increments (DT / Dt) in °C / 100 a calculated for the last 200 years, as functions of depth

| Level | Depth (m) | $T\,(T-T_{Levitus})$ | DT / Dt |
|---|---|---|---|
| 1 | 12.50 | 18.339 (+0.258) | 0.0007 |
| 2 | 37.50 | 17.212 (−0.257) | 0.0011 |
| 3 | 62.50 | 15.971 (−0.555) | 0.0016 |
| 4 | 87.50 | 15.130 (−0.360) | 0.0022 |
| 5 | 112.50 | 14.358 (−0.134) | 0.0027 |
| 6 | 137.50 | 13.778 (+0.272) | 0.0032 |
| 7 | 162.50 | 13.120 (−0.189) | 0.0035 |
| 8 | 187.50 | 12.502 (+0.639) | 0.0039 |
| 9 | 212.50 | 11.937 (+0.056) | 0.0044 |
| 10 | 237.50 | 11.404 (+0.629) | 0.0048 |
| 11 | 262.50 | 10.915 (+0.133) | 0.0052 |
| 12 | 287.50 | 10.465 (+0.571) | 0.0058 |
| 13 | 312.50 | 10.044 (+0.148) | 0.0063 |
| 14 | 341.59 | 9.599 (+0.755) | 0.0070 |
| 15 | 382.84 | 9.120 (+0.653) | 0.0071 |
| 16 | 443.94 | 8.470 (+0.598) | 0.0091 |
| 17 | 531.98 | 7.720 (+0.792) | 0.0106 |
| 18 | 653.23 | 6.760 (+0.799) | 0.0140 |
| 19 | 812.95 | 5.848 (+0.855) | 0.0179 |
| 20 | 1015.24 | 4.781 (+0.669) | 0.0240 |
| 21 | 1262.90 | 3.879 (+0.515) | 0.0274 |
| 22 | 1557.34 | 3.248 (+0.473) | 0.0283 |
| 23 | 1898.57 | 2.829 (+0.522) | 0.0287 |
| 24 | 2285.17 | 2.447 (+0.505) | 0.0269 |
| 25 | 2714.34 | 2.100 (+0.434) | 0.0271 |
| 26 | 3181.98 | 1.724 (+0.307) | 0.0250 |
| 27 | 3682.83 | 1.353 (+0.174) | 0.0269 |
| 28 | 4210.62 | 1.113 (+0.127) | 0.0293 |
| 29 | 4758.26 | 0.968 (+0.074) | 0.0264 |
| 30 | 5318.06 | 1.025 (+0.016) | 0.0128 |
| Average | | 4.080 (+0.415) | 0.0227 |

The isopycnal mixing scheme of GM90 has been adopted to the present model. As shown in Zhang et al. (1996), one of the major problems in the performance of ML20 is the simulated (permanent) thermocline being too thick and too diffuse. The ML20-simulated global and annual mean temperatures below 100 m are significantly higher than the observed values of Levitus (1982) . The maximum error in ML20-0 can reach +2.95 degrees Celsius at the depth of 900 m (see Table 2 in Zhang et al., 1996). It has been found that the modeled thermocline is sensitive to the diffusion process (see Fig. 16 in their paper). The use of the isopycnal mixing scheme in the present model results in essential improvements in both the thermocline and deep ocean temperatures. As shown in Table 2, the errors of temperature at the depths of 812 m, 1015 m, 2285 m, 3181 m and 4210 m are 0.86, 0.67, 0.51, 0.31 and 0.13 degrees Celsius respectively, much less than those in ML20-0 (see Table 2 in Zhang et al., 1996). More detailed comparisons will be given in Section 4.

In addition to experiment D2, several basic experiments named D1, D3, D4, D11, D13 and D14 have also been conducted in order to gain some knowledge on the model's sensitivity to external forcing, sub-grid parameterizations and time integration methods. The chief differences among these experiments are listed in Table 4 where some items such as "reduced wind stress", "Ri-dependent mixing", "solar penetration", etc. will be explained in detail in

**Table 3.** Global and annual mean salinities in psu for the year 1000 and its centennial increments (DS / Dt) in psu / 100 a calculated for the last 200 years, as functions of depth

| Level | Depth (m) | S (S−$S_{Levitus}$) | DS / Dt |
|---|---|---|---|
| 1 | 12.50 | 34.675 (−0.068) | 0.0003 |
| 2 | 37.50 | 34.719 (−0.142) | 0.0003 |
| 3 | 62.50 | 34.789 (−0.151) | 0.0004 |
| 4 | 87.50 | 34.829 (−0.164) | 0.0005 |
| 5 | 112.50 | 34.855 (−0.165) | 0.0005 |
| 6 | 137.50 | 34.892 (−0.143) | 0.0006 |
| 7 | 162.50 | 34.894 (−0.139) | 0.0007 |
| 8 | 187.50 | 34.889 (−0.099) | 0.0007 |
| 9 | 212.50 | 34.881 (−0.107) | 0.0008 |
| 10 | 237.50 | 34.868 (−0.058) | 0.0009 |
| 11 | 262.50 | 34.855 (−0.071) | 0.0009 |
| 12 | 287.50 | 34.842 (−0.025) | 0.0010 |
| 13 | 312.50 | 34.827 (−0.040) | 0.0011 |
| 14 | 341.59 | 34.813 (+0.021) | 0.0012 |
| 15 | 382.84 | 34.794 (+0.030) | 0.0014 |
| 16 | 443.94 | 34.774 (+0.050) | 0.0016 |
| 17 | 531.98 | 34.747 (+0.084) | 0.0019 |
| 18 | 653.23 | 34.737 (+0.119) | 0.0024 |
| 19 | 812.95 | 34.734 (+0.139) | 0.0031 |
| 20 | 1015.24 | 34.753 (+0.141) | 0.0041 |
| 21 | 1262.90 | 34.763 (+0.106) | 0.0046 |
| 22 | 1557.34 | 34.792 (+0.098) | 0.0044 |
| 23 | 1898.57 | 34.808 (+0.086) | 0.0042 |
| 24 | 2285.17 | 34.806 (+0.070) | 0.0037 |
| 25 | 2714.34 | 34.789 (+0.048) | 0.0032 |
| 26 | 3181.98 | 34.759 (+0.020) | 0.0019 |
| 27 | 3682.83 | 34.730 (−0.006) | 0.0004 |
| 28 | 4210.62 | 34.718 (−0.013) | −0.0004 |
| 29 | 4758.26 | 34.712 (−0.016) | −0.0012 |
| 30 | 5318.06 | 34.722 (−0.003) | −0.0024 |
| Average | | 34.770 (+0.046) | 0.0024 |

Section 5. The spin-up integrations of these experiments are illustrated further with a schematic diagram shown in Fig. 1. In this paper, the studies on the modeled mean circulation are based on data of experiment D2, which have been integrated for 1000 years, and some

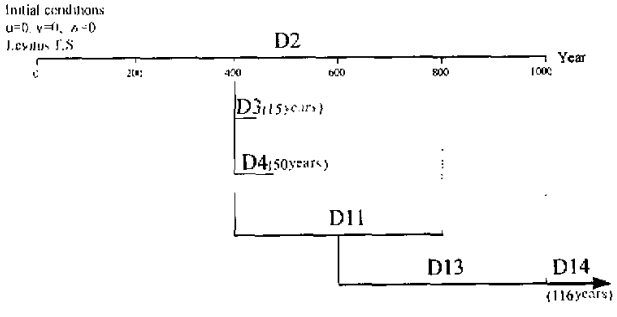


Fig. 1. Schematic diagram for the implementation of basic experiments.

**Table 4.** Some basic experiments and their chief differences

| | Basic Experiments | | | | | | |
|---|---|---|---|---|---|---|---|
| | D1 | D2 | D3 | D4 | D11 | D13 | D14 |
| Isopycnal Mixing | No | Yes | Yes | Yes | Yes | Yes | Yes |
| Reduced Wind Stress | No | No | Yes | Yes | Yes | Yes | Yes |
| Solar Penetration | No | No | Yes | Yes | Yes | Yes | Yes |
| Ri-dependent Mixing | No | No | Yes | Yes | Yes | Yes | Yes |
| Reduced Horizontal Viscosity | No | No | No | Yes[1] | Yes[2] | Yes[2] | Yes[2] |
| Realistic Arctic Bathymetry | No | No | No | No | No | Yes[3] | Yes[3] |
| Synchronous Integration | No | No | No | No | No | No | Yes[4] |
| Integration Time (years) | 700 | 1000 | 15 | 50 | 200 | 400 | 162 |
| Starting Year of Integration | 0 | 0 | 400 of D2 | 400 of D2 | 400 of D2 | 200 of D11 | 400 of D13 |

1. The horizontal viscosity in $m^2/s$, $A_M = 1.0 \times 10^4$ (10°S–10°N), $5.0 \times 10^4$ (30°S–10°S; 10°N–30°N), and $20.0 \times 10^4$ (poleward of 30°).
2. $A_M = 5.0 \times 10^4$ (60°S–50°N) and $20.0 \times 10^4$ (elsewhere).
3. Except the North Pole being treated as an isolated island (Y. Q. Yu, personal communication).
4. The time steps for barotropic and baroclinic modes and tracers are: $\Delta t_B = 2$ min., $\Delta t_C = 4$ h and $\Delta t_T = 8$ h respectively.

comparative studies are based on data of experiments, D1, D3 and D4. The results of experiments D13 and D14, will be given in the future.

## 3. Sea surface temperature (SST), salinity (SSS) and height (SSH), and barotropic transport streamfunction

Fig. 2a shows the modeled annual mean "SST" (at the depth of 12.5 m) and sea-ice distribution. Fig. 2b shows the deviation of the modeled SST from the observation of Levitus (1994). It can be seen in these figures that the large-scale SST and sea-ice patterns are well simulated, reflecting that the SST errors in most of the areas (including fringe areas of sea ice) are less than or around one degree Celsius. Larger errors of SST occur in the eastern equatorial Pacific, southern Indian Ocean, east of Drake Passage, and some continental boundary regions. In particular, the SST errors near the western boundaries of the North Pacific and North Atlantic Oceans between 30°–50°N can reach more than five and three degrees Celsius respectively. These largest errors are common in coarse-resolution models and obviously related to the distorted physics of local heat balance due to underestimated and diffusive boundary currents in such models. In the eastern equatorial Pacific, the modeled SST is two degrees colder between 120°–150°W and one degree warmer in the east of 100°W than observation. As a result, the east-to-west gradient of SST in Niño 1–3 regions becomes

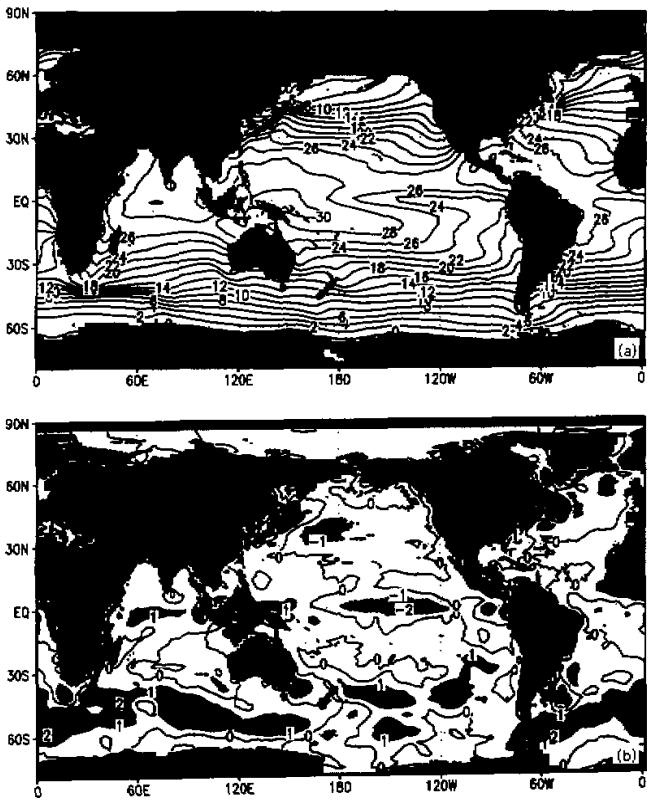


Fig. 2. Annual mean SST (in Celsius) and sea-ice distribution (a) and the deviation of SST from the observation of Levitus (1994) (b).

weaker than the observed one. It will be shown in Section 5 that this kind of errors can be partly reduced by improving the simulated equatorial thermocline.

Figs. 3a and 3b show the simulated annual mean sea surface layer salinity (SSS) and its deviation from the observation of Levitus (1994) respectively. It is obvious that the good agreement in SSS pattern between simulation and observation results from using the restoring boundary condition (rather than the realistic fresh-water flux condition) in the present phase of the model's integration. However, the deviation pattern, which will be used in interpreting the "fresh-water flux" for the second phase of the model's integration with the so-called "mixed" boundary condition (Bryan, 1986), is quite similar to the observed fresh-water flux (Zhou et al., 1998). The physical reason for this, if there is any, requires further investigation.

The modeled sea surface height (SSH), which has been one of the prognostic variables of IAP / LASG ocean models without using the rigid-lid approximation, is shown in Fig. 4a. With the meridional grid size of about 2 degrees, the model can depict an anticyclonic curvature between the two troughs in the equatorial Pacific Ocean. In fact, the anticyclonic curvature corresponds to the model's North Equatorial Counter Current (NECC) which is weaker than the reality (the figure is not shown). Such a detailed structure in the modeled SSH is

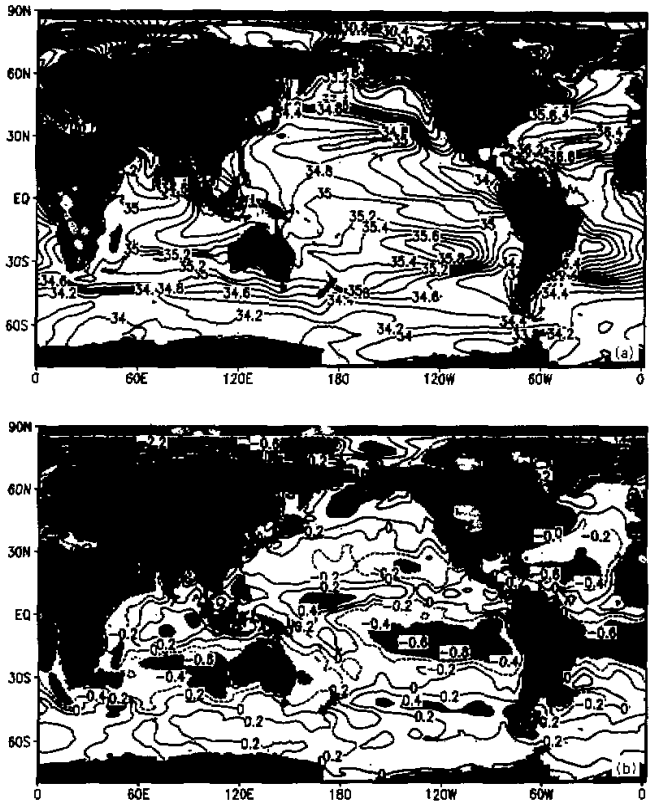


Fig. 3. Annual mean surface layer salinity in psu (a) and its deviation from the observation of Levitus (1994) (b).

quite sensitive to the horizontal viscosity. In fact, as shown in Fig. 4b, the anticyclonic curvature near the equator becomes sharper and moves further westward in experiment D4 with reduced horizontal viscosity in the tropical oceans (see Section 5).

The large poleward down-gradient of SSH around the Antarctica is noticeably correlated to the Antarctic Circumpolar Current (ACC) as seen from the barotropic transport streamfunction (Fig. 5). In comparison with ML20, the transports of both the Kuroshio-like and Gulf-like western boundary currents are significantly enhanced. However, the modeled volume transport through Drake Passage is now only 70 Sv which is considerably weaker than not only observation (about 130 Sv, see Covey, 1994) but also that simulated by ML20-0 (about 100 Sv). In fact, with the initial conditions of temperature and salinity given by the three-dimensional data of Levitus (1994), the initial value of the transport through Drake Passage approximates to its observational estimate of 130 Sv (the figure is not shown). However, with the whole water column in the extreme Southern Oceans getting evidently warmer than observation in the process of integration (compare Figs. 6c and 6a), the strength of the ACC becomes dramatically weakened. It follows that the volume transport of ACC may be driven not only by the surface wind stress but also by the density differentials in the

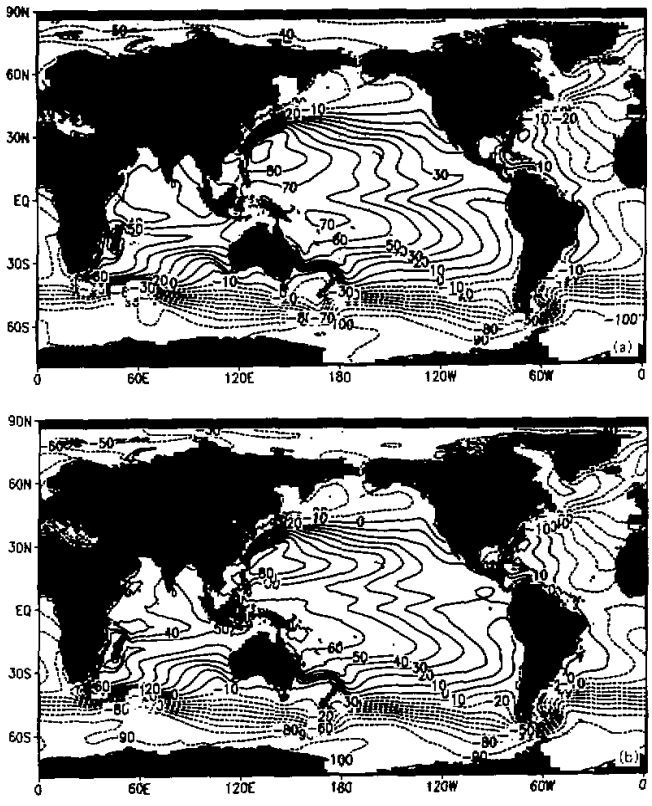


Fig. 4. Annual mean sea surface height in cm (a) and its counterpart with reduced horizontal viscosity in experiment D4 (b).

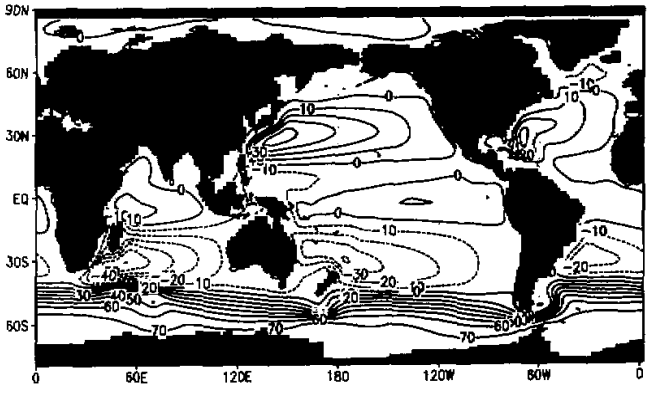


Fig. 5. Annual mean barotropic transport streamfunction in Sv.

internal oceans. A possible reason for the warming bias in the model's Southern Oceans will be discussed in the next section.

## 4. Permanent thermocline, thermohaline circulation (THC), and meridional heat transport (MHT)

Danabasoglu et al. (1994) have shown promising results of their experiments using a parameterization for mesoscale eddy-induced mixing, i. e. the so-called isopycnal mixing. Compared with the conventional mixing scheme, the isopycnal mixing scheme gives a sharper thermocline, colder deep ocean, and stronger meridional transport of heat. As shown in follows, it is also the case for the present ocean model if the isopycnal mixing scheme is used.

Fig. 6a shows the climatological annual mean globally and zonally averaged potential temperature based on the data of Levitus (1982), while Figs. 6b and 6c represent the simulated ones of ML20-1 and experiment D2 respectively. It is obvious that the thermocline modeled by ML20-1 is much thicker than observation although the shape of zonal mean temperature is generally in agreement with the observed one. Moreover, the modeled high-latitude temperatures below the surface layer are also higher than the observed ones. below the depth of 100 m, for instance, the temperatures around 60°N are more than one degree warmer than observation. Similar features can also be found in the extreme Southern Oceans.

Compared with the result of ML20-1, the most outstanding feature in experiment D2 is that the thermocline becomes sharper. For instance, the bottom of isotherm for 4°C is just below the depth of 1000 m, which is quite similar to observation, while that modeled by ML20-1 is below the depth of 2000 m, which is far from the reality. The improved zonal mean temperature stratification is near-perfect, i.e. no longer higher than the observed one within and below the thermocline as that of ML20-1. The improved new features can also be found in the simulated northern high-latitude temperatures below the surface layer. The original exhibition of downward and poleward expansion of the isotherms in the northern high-latitudes as shown in ML20-1 is vanished in the new model.

The reason for the improvements in zonal mean temperature simulation is likely the use of isopycnal mixing process although the present model is different from ML20-1 in many aspects particularly in the spatial resolutions. In order to further confirm this, experiment D1 has been conducted without using the isopycnal mixing scheme. The figure (not shown here) is almost the same as Fig. 6b. These comparisons clearly show that the isopycnal mixing scheme is much beneficial to the simulation of permanent thermocline in coarse resolution oceanic general circulation models.

As has been mentioned in Section 3, an noticeable bias of the zonal mean temperature simulated by the new model appears in the extreme Southern Oceans where the modeled temperature is generally higher than observation and even the error can reach about one degree below the depth of 800 m. A possible reason for this bias may be the underestimate of the extreme southern cell in the modeled thermohaline circulation.

The zonal mean meridional overturning streamfunction for the World Ocean and the Atlantic Ocean simulated by ML20-1 is shown in Figs. 7a and 7b respectively. Figs. 8a and 8b are the corresponding results of experiment D2. Both of the two models can simulate the large scale oceanic circulation successfully to certain degrees. For instance, in the surface waters, two nearly symmetrical Ekman cells are formed on either side of the equator, while a third surface cell, termed the Deacon Cell, can be seen northward of ACC, which is originally driven by surface wind stress and can downwell to a great depth due to the unique dynamical

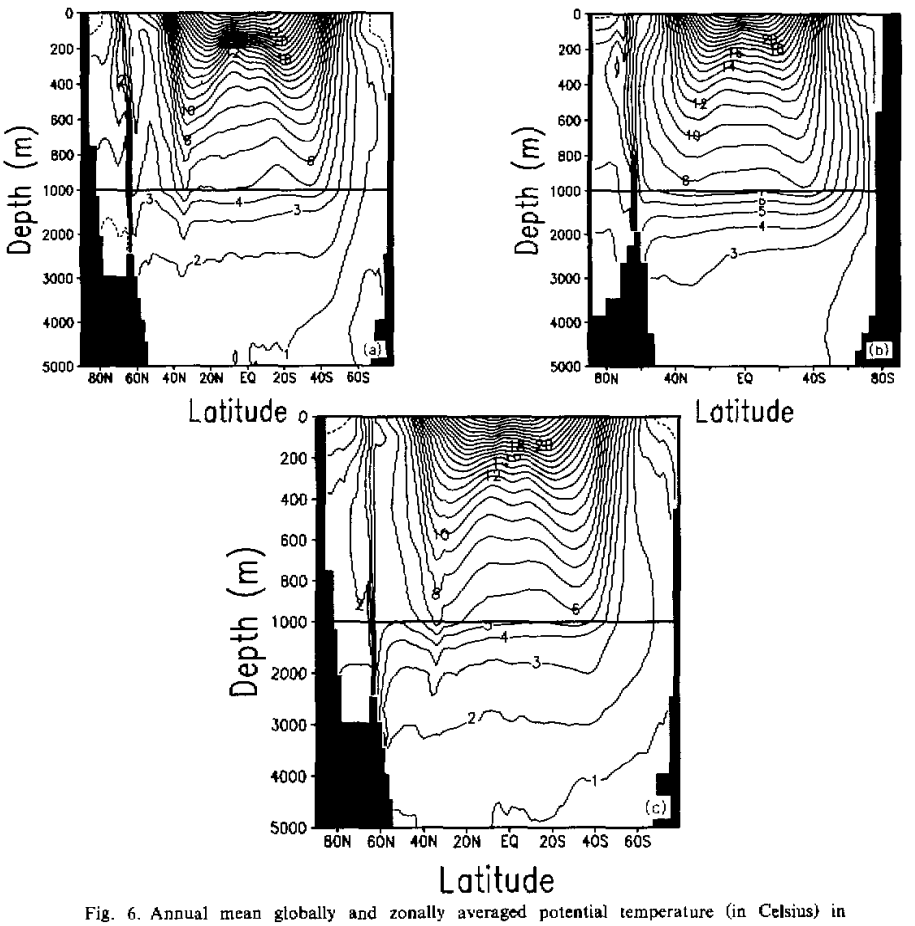


Fig. 6. Annual mean globally and zonally averaged potential temperature (in Celsius) in climatological data of Levitus (1994) (a), ML20-1 (b), and D2 (c).

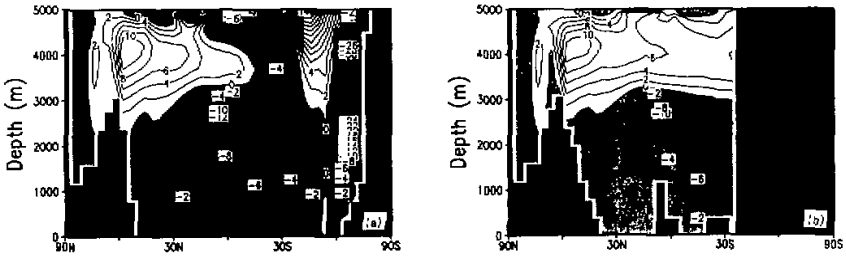


Fig. 7. Zonal mean meridional overturning streamfunction for the World Ocean (a) and Atlantic Ocean (b) simulated by ML20-1.

constraints of the Drake Passage gap. The most important member of the global thermohaline circulation, NADW, and the associated cross-equatorial outflow can also be

clearly seen in simulations of the two models although their strengths are significantly different in the two simulations.

Although ML20–1 is capable of simulating the major features of the thermohaline circulation, as shown in Fig. 7, there are still some demerits. One of them is that the modeled rate of the NADW outflow, defined as the transport of water of North Atlantic across the latitude at the southern tip of Africa, is only about 5 Sv. It seems that the NADW outflow is not strong enough, so that its flow further south can only be seen in Fig. 7b but not in Fig. 7a.

Encouraging improvements can be seen in the results of experiment D2. First, the modeled rate of the NADW outflow can reach about 10 Sv (see Fig. 8b), which is one time stronger than that of ML20–1. The flow which lies to the further south of NADW outflow can be seen not only in Fig. 8b but also in Fig. 8a, although still a little weak in Fig. 8a.

It should be noted that the extreme Southern Ocean cell, of which the downwelling branch is considered as the major source of Antarctic Bottom Water (AABW), in experiment D2 (see Fig. 8a) is far less than the values given by both England (1993) and ML20–1 (Fig. 7a), in which some artificially enhanced salinity forcings were used in imitating the effect of brine rejection around Antarctica continent. The detrimental impact of artificially enhanced salinity forcing in ML20 is that deep convection occurs in many places, much more extensively than is known to occur in nature (for ML20–0, see Fig. 11 of Zhang et al., 1996). In experiment D2, the convection occurs only in a few small areas around Antarctica (the figure is not shown), mainly located in the Weddell and Ross seas where deep-water formation has been observed. While the location of deep convection becomes more realistic, the underestimate of the extreme Southern Ocean cell is still a demerit of the new model, which may result in the deep and bottom waters there being evidently warmer than observation as shown in Fig. 6, and consequently the underestimated ACC.

In reality, two distinct forms of deep water formation are recognized around the Antarctica: near-continent and open sea convections. The former involves one of two processes:

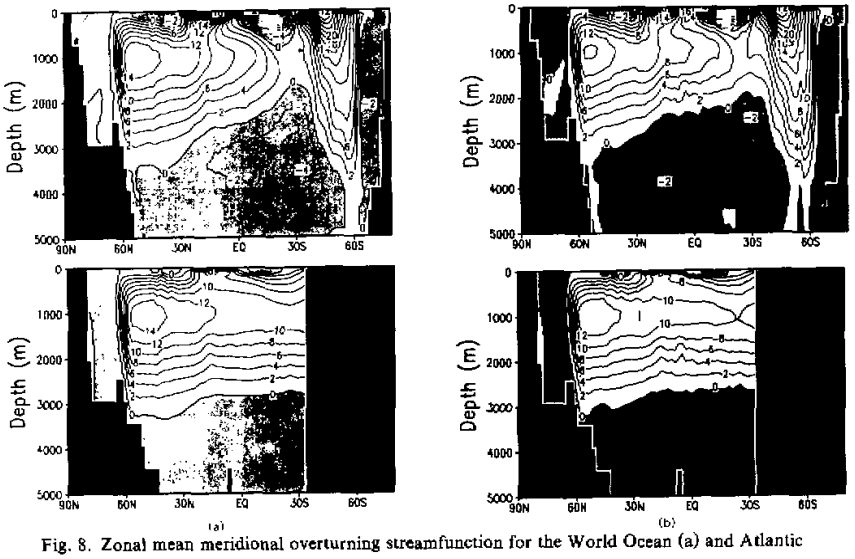


Fig. 8. Zonal mean meridional overturning streamfunction for the World Ocean (a) and Atlantic Ocean (b) in experiment D2, and that for the World Ocean in experiment D4 (c).

intense evaporation or more typically brine rejection above the continental shelf produces dense heavy water which sinks down and along the continental shelf slope under the combined forces of gravity, friction and Coriolis force (Killworth, 1983); alternatively supercooled water may be formed at the base of a thick ice shelf during freezing or melting and this dense water may in turn flow down-slope (Grumbine, 1991). Since this kind of descending continental slope process cannot be reproduced and only the open sea convection processes are involved in the present model, the underestimate of extreme Southern Ocean cell seems unavoidable.

The zonally-vertically integrated annual mean northward heat transport for the World Ocean and the Atlantic Ocean in ML20-1 is shown in Fig. 9, while the corresponding results of experiment D2 are shown in Fig. 10a (for the World Ocean) and Fig. 10b (for the Atlantic) respectively. Although the general pattern of the meridional heat transport shown in Fig. 9 is in agreement with observation (see Fig. 3a of Gleckler et al., 1994), there still exist some discrepancies. First, there is a distorted curl between 60°S and 30°S in the Southern Oceans; Second, the magnitude of northward heat transport in the Atlantic Ocean, which is closely related to the strength of NADW, is evidently less than the observed estimate of Hastenrath (see Fig. 40 of Weaver et al., 1992). Just as aforementioned, this may be attributed to the underestimate of the modeled NADW in ML20-1.

Promising improvements can be found in Fig. 10. The distorted curl in the Southern Ocean, as seen in Fig. 9, no longer exists, and following the enhancement of NADW, the northward heat transport in the Atlantic Ocean increased significantly, reflecting that its value at the equator is about 0.6 PW and its maximum can almost reach 0.9 PW, both evidently greater than that of ML20-1. Again, the improvements in the simulation of MHT should also be resulted from using the isopycnal mixing scheme in the present model. In fact, the MHT simulated in experiment D1 using the ordinary down-gradient mixing instead of the isopycnal mixing, as shown by the dashed lines in Fig. 10, exhibits the demerits quite similar to those of ML20-1.

## 5. Impact of horizontal viscosity on simulation of equatorial thermocline and undercurrent, as well as THC

As discussed in Section 4, by the use of GM90 isopycnal mixing scheme, the permanent thermocline is reproduced well. However, the simulated equatorial thermocline, is still not captured well by the model. Fig. 11 shows the vertical cross-section of annual mean temperature along the equator in experiment D2 and observation (Levitus, 1994). Compared with the observed one, the model's warm pool is too shallow, cold tongue too strong, and thermocline too diffusive.

A series of numerical experiments have been carried out aimed at improving the simulation of equatorial thermocline. In one experiment the observational wind stress of Hellerman and Rosenstein (1983), which is considered to be overestimated in the tropical ocean (Stockdale et al., 1993), is reduced by 30% at the equator and recovered linearly to its normal values at 30°N and 30°S. It turns out that the thermocline remains largely unchanged although the surface cold tongue is improved especially in Niño 3 region (the figure is not shown here). In experiment D3, besides using the reduced wind stress, another two physical processes are considered, i.e (a) the penetration of solar radiation (about 14% energy penetrates directly into the second layer in this model); (b) Richardson number (Ri) dependent mixing in the tropical oceans from 30°S to 30°N (Pacanowski et al., 1981). Compared with the

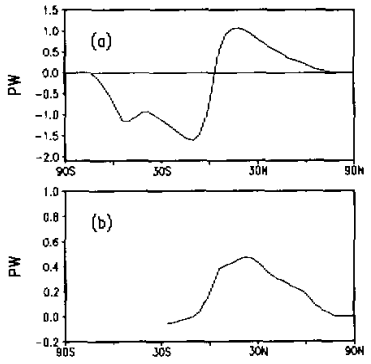


Fig. 9. Zonally-vertically integrated annual mean *northward heat transport* (in PW) for the World Ocean (solid line) and the Atlantic Ocean (dashed line) in ML20-1.

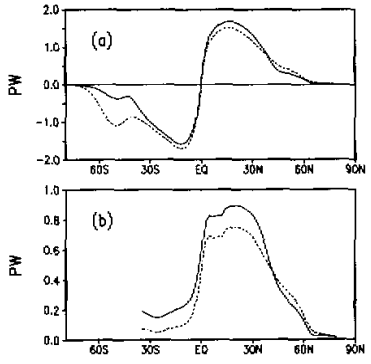


Fig. 10. Zonally-vertically integrated annual mean *northward heat transport* (in PW) in the World Ocean (a) and Atlantic Ocean (b) for experiment D2 (solid line) and D1 (dashed line).

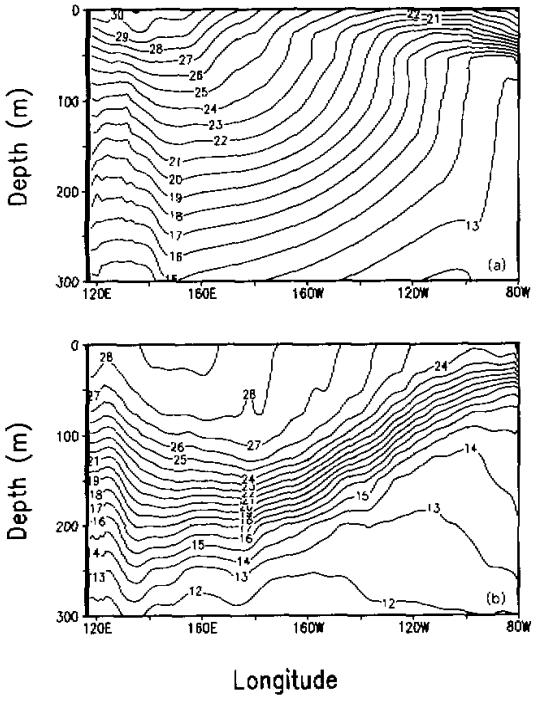


Fig. 11. Longitude-depth cross-section of annual mean temperature along the equator in experiment D2 (a) and observation (Levitus, 1994) (b).

results of D2, the simulated subsurface structure of both warm pool and cold tongue in experiment D3 is improved but the equatorial thermocline is still too diffuse (the figure is not shown here).

It is recognized that both the surface current and sub-surface current have important impact on the three-dimensional structure of temperature in the upper tropical oceans. It appears, however, the simulated equatorial undercurrents in above experiments are too weak, of which the maximum is only about 15 cm / s (the figure is not shown), almost one order of magnitude smaller than the observed one. As discussed by Maes et al. (1997), the simulation of equatorial undercurrent is very sensitive to lateral eddy viscosity coefficient (see their Fig. 5). The larger the lateral viscosity coefficient, the weaker the undercurrent. In the above experiments, the horizontal viscosity coefficient is set to $20 \times 10^4$ m$^2$ / s to guarantee the computational stability in the spin-up phase. In experiment D4, with smaller lateral viscosity coefficients being used in the tropical oceans ($1.0 \times 10^4$ m$^2$ / s between 10°S and 10°N, see Table 2 for details), the model has been re-run for 50 years started from the 400th model year of D2. The result shows that the simulated equatorial thermocline in the equatorial regions is improved greatly, reflecting that a west-east tilted front zone associated with a strong gradient of temperature ranging between 24-14°C can be clearly identified (see Fig. 12a), which is similar to observation but cannot be found in experiment D2. Meanwhile the maximum of equatorial undercurrent increases to 55 cm / s (see Fig. 12b), which is an acceptable value for such a coarse-resolution model.

The above experiments indicate that the structure of temperature within the equatorial thermocline is dominated by the advection rather than the mixing process, which is different from the case for the permanent thermocline. This is just the reason why the use of isopycnal mixing scheme in experiment D2 has no positive contribution to the improvement of equatorial thermocline. Instead, the simulation of equatorial thermocline is improved significantly while the upper ocean currents are improved by using a reduced viscosity as shown in experiment D4.

In a coarse-resolution ocean model, the so-called " viscosity" is nothing but a parameterized representation for the sub-grid scale mixing process in current fields. Therefore a more effective way to improve the simulations of upper-layer currents as well as equatorial thermocline is to increase model's resolution, especially in horizontal directions. And this is perhaps one of the reasons for increasing the grid sizes near the equator in many ocean models used in simulation or prediction of ENSO events. In fact, refinement of resolution seems to be necessary not only in the tropical oceans but also in, for instance, the western boundary regions where the advective process is crucial to the heat transport and thereby local structure of temperature and salinity. For global ocean models, however, it is still worth putting some effort in searching for more reasonable paramterization schemes for sub-grid scale viscosity due to limitations of computer resources.

Another interesting phenomenon is that the strength of the modeled thermohaline circulation is weakened while the simulation of equatorial thermocline is improved with the reduced viscosity, reflecting the NADW overturning rate in experiment D4 is about 2 Sv less than in experiment D2 (see Fig. 8c). Comparing Fig. 11a with Fig. 12a, we can find that the weakening of the thermohaline circulation in experiment D4 is likely to be resulted from the decrease of pole-to-tropics density difference associated with the sharper equatorial thermocline.

It is reasonable to speculate that the change of the equatorial thermocline in the tropical Atlantic (rather than Pacific) is the direct reason accounted for the decrease of NADW in experiment D4. An additional experiment, which is the same as experiment D4 except that the treatment in the Atlantic is remained the same as in experiment D2, is carried out for 50 years.

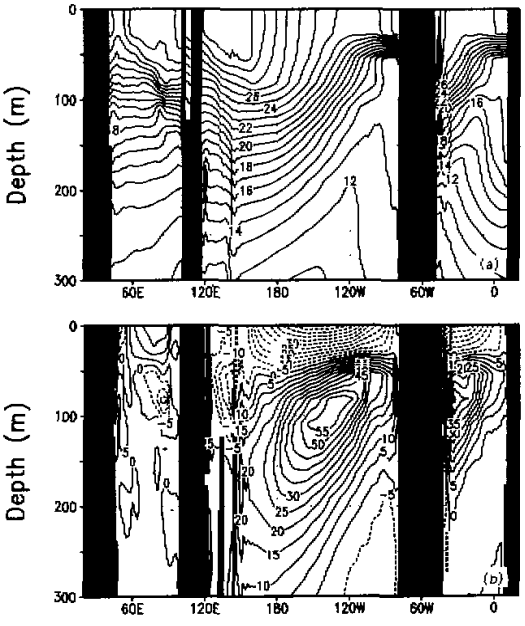


Fig. 12. Longitude–depth cross-section of annual mean temperature (a) and zonal current velocity (positive eastward) (b) along the equator in experiment D4.

The result indicates that the modeled equatorial thermocline in the tropical Pacific is improved as shown in experiment D4 while the equatorial thermocline in the tropical Atlantic as well as NADW remain unchanged in comparison with experiment D2 (the figure is not shown here). Thus it confirms that the change of NADW in experiment D4 is largely due to change of the equatorial thermocline in the tropical Atlantic. An implication of this experiment is that the possible variability of the equatorial thermocline in the tropical Pacific may have no direct impact on the thermohaline circulation (at least on decadal and interdecadal time scales), although the thermohaline circulation is commonly regarded as a global conveyer belt.

## 6. *Concluding remarks*

This paper reports the fundamental framework and some experiments of the third generation of IAP / LASG world ocean general circulation model, which is designed and performed based on the previous twenty-layer model (ML20) but with remarkably enhanced spatial resolutions and some improved parameterizations.

The model has been integrated for more than 1000 years with seasonally varying climatological surface forcing. Preliminary analyses show some encouraging improvements in comparison with ML20. The adoption of the isopycnal mixing scheme of GM90 in the new model goes to promising results: the permanent thermocline becomes sharper, the deep ocean

becomes colder, the rate of NADW outflow becomes stronger and the meridional heat transport becomes larger than those simulated by ML20.

Sensitivity experiments aimed at improving the simulation of equatorial thermocline have revealed that the upper ocean current fields have important impact on the structure of temperature of the thermocline. The simulation of equatorial undercurrent is quite sensitive to lateral eddy viscosity. A smaller lateral viscosity coefficient used in the tropical oceans leads to a greatly improved simulation of the equatorial undercurrent and consequently the equatorial thermocline. Corresponding experiments indicate that the intensity of NADW can be affected by changing the horizontal viscosity in the equatorial Atlantic Ocean through changing the temperature structure in the equatorial thermocline. On the other hand, the possible variability of the equatorial thermocline in the tropical Pacific may have no direct impact on the thermohaline circulation.

While some important improvements have been achieved in the new generation of IAP / LASG ocean models, there are still some problems in the present simulation. Among them, the considerable underestimate of the volume transport of ACC may be the most noticeable one. A preliminary analysis indicates that the underestimate seems to be related to lacking deep and bottom water formation in Weddell and Ross Seas, which results in the baroclinity in the Southern Oceans being much weaker than observation. Further exploration in this regard is needed.

Since the model will be coupled with a T63 AGCM to provide boundary conditions for a high-resolution Pacific-Indian Ocean model (Zhao et al., 1998) to conduct SST forecasts, it is necessary to assess the ability of this model in simulating SST variability. Recently, some experiments on the model's response to observed wind stresses for the time period of 1980's were conducted by Yu and Izard (personal communication). It is encouraging that the model SST anomalies (SSTAs) during 1982-1983 and 1986-1987 El Niño events are significant and reasonable although the magnitudes of SSTAs are still underestimated compared to those given by the NCEP ocean data assimilation system (Ji, et al., 1995; Behringer et al., 1998). The paper of Yu and Izard is in preparation and some further investigations on the structure of the model equatorial circulation system and its relationship with El Niño events will be reported in the near future.

This work is supported by "National Key Project Studies on Short-range Climate Prediction System in China" (NO.96-908-02-03) and the "National Climbing Project Studies on Climate Dynamics and Climate Prediction Theory" (C95-P-21). All of the experiments were run on the SGI / Origin 2000 high performance computer at the State Key Laboratory of Numerical Modeling for Atmospheric Sciences and Geophysical Fluid Dynamics (LASG), Institute of Atmospheric Physics (IAP).

The authors would like to thank Drs. Zhou, G.-Q. and Li, Xu for some helpful discussions on the equatorial thermocline. The lion's share of thanks goes to Dr. Yu, Y.-Q., who has extended the northern boundary of the model to Arctic Pole and conducted experiment D13 and D14.

## REFERENCES

Asselin, R., 1972: Frequency filter for time integrations. *Mon. Wea. Rev.*, **100(6)**, 487-490.

Behringer, D. W., M. Ji, and A. Leetmaa, 1998: An improved coupled model for ENSO prediction and implication for ocean initialization. Part I: The ocean data assimilation system. *Mon. Wea. Rev.*, **126**, 1013-1021.

Bryan, F., 1986: High-latitude salinity and interhemispheric thermohaline circulation. *Nature*, **323**, 301-304.

Bryan, K., and M. D. Cox, 1972: An approximate equation of state for numerical models of ocean circulation. *J. Phys. Oceanogr.*, **2**, 510-514.

Bryan, K., 1984: Accelerating the convergence to equilibrium of ocean-climate models. *J. Phys. Oceanogr.*, **14**, 666-673.

Chen, K. M., 1994: Improvement on IAP coupled ocean-atmosphere general circulation model and simulation of gradually increasing $CO_2$ induced climate change, Ph. D. Thesis, Institute of Atmospheric Physics, Chinese Academy of Sciences (in Chinese).

Chen, K. M., X. H. Zhang, and Q. C. Zeng, 1993: Features of interannual variability in a coupled ocean-atmosphere general circulation model, in Climate Variability. *Proceedings of International Workshop on Climate Variabilities (IWCV)*, edited by Ye Duzheng et al., China Meteorological Press, Beijing, 1993, 255-272.

Chen, K. M., X. H. Zhang, and X. Z. Jin, 1997: A coupled ocean-atmosphere general circulation model for studies of global climate changes, I. Formulation and performance of the model. *Acta Oceanologica Sinica*, **19(3)**, 21-32. (in Chinese)

Covey, C., 1994: Global ocean circulation and equator-pole heat transport as a function of ocean GCM resolution, Report No.19, Program for Climate Model Diagnosis and Intercomparison (Lawrence Livermore National Laboratory, Livermore, CA), 30 pp.

Danabasoglu, G., J. C. McWilliams, and P. R. Gent, 1994: The role of mesoscale tracer transports in the global ocean circulation. *Science*, **264**, 1123-1126.

da Silva, A. M., C. C. Young, and S. Levitus, 1994: Atlas of Surface Marine Data 1994, Vol.1: Algorithms and Procedures, NOAA Atlas NECDIS 6, U.S. Dept. of Commerce, Washington, DC, 83 pp.

England, M. H., 1993: Representing the global-scale water masses in ocean circulation models. *J. Phys. Oceanogr.*, **19**, 1730-1752.

Gent, P. R., and J. C. McWilliams, 1990: Isopycnal mixing in ocean circulation models. *J. Phys. Oceanogr.*, **20**, 150-155.

Gleckler, P. J., D. A., Randall et al., 1994: Cloud-radiation effects on implied oceanic energy transports as simulated by atmospheric general circulation models. *Geophys. Res. Lett.*, **22(7)**, 791-794.

Grumbine, R. W., 1991: A model of the formation of high-salinity shelf water on polar continental shelves. *J. Geophys. Res.*, **96(C)**, 22049-22062.

Guo, Y. F., Y. Q., Yu, K. M., Chen, X. Z., Jin, and X. H., Zhang, 1996: Mean climate state simulated by a coupled ocean-atmosphere general circulation model. *Theor. and Appl. Clim.*, **55(1-4)**, 99-112.

Haney, R. L., 1971: Surface thermal boundary condition for ocean circulation models. *J. Phys. Oceanogr.*, **1**, 241-248.

Hellerman, S., and Rosenstein, M., 1983: Normal monthly wind stress data over the world ocean with error estimates. *J. Phys. Oceanogr.*, **13**, 1093-1104.

Ji, M., A. Leetmaa, and J. Derber, 1995: An Ocean Analysis System for Seasonal to Interannual Climate Studies. *Mon. Wea. Rev.*, **123**, 460-481.

Killworth, P. D., 1983: Deep convection in the world ocean. *Reviews of Geophysics and Space Physics*, **21(1)**, 1-26.

Levitus, S., 1982: Climatological Atlas of the World Ocean. NOAA Professional Paper 13, U. S. Government Printing Office, Washington, D. C., 173 pp.

Levitus, S., T. P., Boyer, 1994: World Ocean Atlas 1994: Temperature and Salinity, U. S. Department of Commerce, Washington, D. C.

Liu, H., X. Z. Jin, X. H. Zhang, and G. X. Wu, 1996: A coupling experiment of an atmosphere and ocean model with a monthly anomaly exchange scheme. *Adv. in Atmos. Sci.*, **13(2)**, 133-146.

Maes, C., G. Mades, and P. Delecluse, 1997: Sensitivity of an equatorial Pacific OGCM to the lateral diffusion. *Mon. Wea. Rev.*, **125**, 958-971.

Marotzke, J., 1991: Influence of convective adjustment on the stability of the thermohaline circulation. *J. Phys. Oceanogr.*, **21**, 903-907.

Mellor, G. L., 1993: User's guide for a three-dimensional, primitive equation, numerical ocean model. Princeton University, 1993, 35 pp.

Mesinger, F., and Janjic, Z. I., 1985: Problems and numerical methods of the incorporation of mountains in atmospheric models. *Lectures in Applied Mathematics*, **22**, 81-120.

Pacanowski, R. C., and G., Philander, 1981: Parameterization ofvertical mixing in numerical models of the tropical

ocean. *J. Phys. Oceanogr.*, **11**, 1442–1451.

Parkinson, C. L., and Washington, W. M., 1979: A large-scale numerical model of sea ice. *J. Geophys. Res.*, **84**, 311–337.

Rosati, A and K., Miyakoda, 1988: A general circulation model for upper ocean circulation. *J. Phys. Oceanogr.*, **18**, 1601–1626.

Stockdale, T.. D. Anderson, M. Davey, P. Delecluse, A. Kattenberg, Y. Kitamura, M. Latif, T. yamagata, 1993: Intercomparison of tropical ocean GCMs, TOGA Numerical Experimentation Group, WMO / TD–No. 545.

UNESCO, 10th report of the joint panel on oceanographic tables and standards. UNESCO Tech. Papers in Marine Sci. No. 36, Paris, 1981.

Weaver. A. J., and T. M. C., Hughes, 1992: Stability and variability of the thermohaline circulation and its link to climate, $C^2$GCR Report No. 92–5, McGill Univ., 56 pp.

Wu, G. X., H. Liu, Y. C. Zhao, and W. P. Li, 1996: A nine-layer atmospheric general circulation model and its performance. *Adv. in Atmos. Sci.*, **13(1)**, 1–18.

Wu, G. X., X. H. Zhang, H. liu, Y. Q. Yu, X. Z. Jin, Y. F. Guo, S. F. Sun, W. P. Li, B. Wang, G. Y. Shi, 1997: Global ocean–atmosphere–land system model of LASG(GOALS / LASG) and its performance in simulation study. *Quarterly Journal of Applied Meteorology*, Vol. 8, Supplement Issue, 15–28 (in Chinese).

Yu, R. C., 1989: Design of the limited area numerical weather prediction model with steep mountains. *Scientia Atmospherica Sinica*, **13(2)**, 139–149 (in Chinese).

Yu, Y. Q., and Y. F. Guo, 1995: The interannual variability of climate in a coupled ocean–atmosphere model. *Adv. in Atmos. Sci.*, **12(3)**, 273–288.

Yu, Y. Q., 1997: Design of ocean–sea ice–atmosphere coupling scheme and numerical simulation of interdecadal climate variability, Ph. D. Thesis, Institute of Atmospheric Physics, Chinese academy of Sciences, 130 pp.

Yu, Y. Q., and A. Izard, 1998: Response of an OGCM to the observed wind stress (in preparation).

Zeng, Q. C., and X. H. Zhang, 1987: Available energy conserving schemes for primitive equations on spherical baroclinic atmosphere, *Chinese Journal of Atmospheric Sciences*, **11(2)**, 121–142.

Zeng, Q. C., Zhang, X. H., Liang, X. Z., Yuan, C. G., and Chen, S. F., 1989: Documentation of IAP Two-Level Atmospheric General Circulation Model. DOE / ER / 60314–H1, TR044, Feb. 1989, 383 pp.

Zhang, X. H., and Liang, X. Z., 1989: A numerical world ocean general circulation model. *Adv. in Atmos. Sci.*, **6(1)**, 43–61.

Zhang, X. H., N. Bao, and W. Q. Wang, 1991: Numerical simulation of seasonal cycle of world oceanic general circulation, In the Proceedings of the Sixth Japan and East China Sea Study Workshop (JECSS–VI), Fukuoda, Japan, April 22–27, 1991. (in La mer, 1993, 30, 73–82).

Zhang, X. H., Bao, N., Yu, R. C., and Wang, W. Q., 1992: Coupling scheme experiments based on an atmospheric and an oceanic GCM. *Chinese J. of Atmos. of Sci.*, **16(2)**, 129–144.

Zhang, X. H., K. M. Chen, X. Z. Jin, W. Y. Lin, and Y. Q. Yu, 1996: Simulation of thermohaline circulation with a twenty-layer oceanic general circulation model. *Theoretical and Applied Climatology*, **55(1–4)**, 65–87.

Zhao, Q. G., Y. J., Song, and S. Y., Peng, 1998: Response of interannual variability of SST in tropical Pacific and its sensitivity experiments. *Quarterly Journal of Applied Meteorology*, **9**, 48–58 (in Chinese).

Zhou, T. J., X, H., Zhang, and S. W., Wang, 1998: Aspects of the ocean component of global water cycle evaluated from NCEP / NCAR reanalysis dataset, (to be published in Chinese Acta Meteorologica Sinica).